

Eero Prusti

NUMERICAL STUDIES ON SUPERCONTINUUM OPTIMIZATION

Bachelor's thesis
Faculty of Engineering and Natural Sciences
Examiner: Assoc. Prof. Marco Ornigotti
May 2024

ABSTRACT

Eero Prusti: Numerical studies on supercontinuum optimization
Bachelor's thesis
Tampere University
Science and engineering
May 2024

Supercontinuum generation (SCG) is a process where the spectrum of a narrowband optical pulse experiences extreme broadening. SCG is an active area of research with applications in many areas such as metrology, optical communications and bioimaging. Recent advancements with light sources and waveguides have enabled SCG research to achieve the process more efficiently, and with preferable results. Increase in the computing power of computers has also improved the possibilities of numerical study of supercontinua.

Since supercontinuum generation follows from complex nonlinear interactions and is governed by the General nonlinear Schrödinger equation (GNLSE), its analytical study can be difficult. To overcome this difficulty one can implement a numerical alternative to the task. Using a numerical method not only facilitates the closely analytical study, but also brings a more versatile method as opposed to laboratory testing.

This thesis introduces a numerical method for inspecting the properties of supercontinuum with spectral phase modulation. The numerical approach solves the GNLSE by using the general split-step Fourier method (SSFM) and optimizes the results using a general optimization method. The simulations were conducted with MATLAB.

The numerical method models a hyperbolic secant pulse with a peak power of 10 kW propagating in a photonic crystal fiber with a length of 10 mm. The pulse wavelength is centered around 835 nm with a full width half maximum (FWHM) of 50 fs. The spectral phase of the pulse is expanded to its Taylor series and terms up to the 9th are examined. Each of the terms are studied first individually and then with respect to others.

Using a specific spectral phase on the input pulse resulted in an increase of over 2x in the peak power and a decrease of same magnitude in the FWHM of the output pulse compared to a pulse with a flat spectral phase. Power carried by specific wavelengths were also able to be more than doubled or alternatively reduced to near zero. The changes in the power carried by wavelengths were found to be dissimilar among different wavelengths.

Keywords: supercontinuum generation, split-step Fourier method, spectral phase, generalized nonlinear Schrödinger equation

The originality of this thesis has been checked using the Turnitin OriginalityCheck service.

TIIVISTELMÄ

Eero Prusti: Superjatkumon optimoinnin numeerinen tutkiminen

Kandidaatintyö

Tampereen yliopisto

Teknis-luonnontieteellinen

Toukokuu 2024

Superjatkumon generoiminen on prosessi, missä kapeaspektrisen optisen pulssin spektriä laajennetaan merkittävästi. Superjatkumot ovat aktiivinen tutkimuksen kohde, ja niitä pystytään käyttämään monilla eri tekniikan osa-alueilla, kuten metrologiassa, optisessa tiedonsiirrossa ja biokuvantamisessa. Viimeaikaiset kehitykset aaltojohteiden ja valonlähteiden tutkimuksessa ovat mahdollistaneet superjatkumojen tehokkaamman tutkimisen. Myös tietokoneiden laskentatehon nousu on lisännyt superjatkumojen tutkimisen mahdollisuuksia.

Koska superjatkumon muodostuminen on seurausta monesta epälineaarista vuorovaikutuksesta, ja se noudattaa yleistettyä epälineaarista Schrödingerin yhtälöä (GNLSE), sen puhdas teoreettinen tutkiminen on hyvin vaikeaa. Tutkimisen mahdollistamiseksi voidaan ottaa käyttöön numeerisia menetelmiä. Numeeristen menetelmien etuna on myös niiden monikäyttöisyys käytännön laboratoriotutkimukseen verrattuna.

Tässä opinnäytetyössä superjatkumon muodostamista ja ominaisuuksia tutkitaan numeerisen menetelmän avulla. Superjatkumon kehitykseen vaikutetaan muuttamalla alkupulssin taajuusvaihetta. GNLSE ratkaistaan käyttäen split-step Fourier menetelmää, ja optimointi suoritetaan yleisellä optimointimenetelmällä.

Numeerisella menetelmällä mallinnetaan hyperbolista sekanttipulssia, jonka huipputeho on 10 kW. Pulssin eteneminen tapahtuu 10 mm pituisessa fotonisessa kristallijohteessa. Pulssin puolivoleveys (FWHM) on 50 fs ja sen keskiaallonpituus on 835 nm. Pulssin taajuusvaihe muunnetaan Taylorin sarjaksi, josta tutkitaan termejä kahdeksanteen termiin asti. Jokaista vaihetermiä tutkitaan itsenäisesti sekä yhdessä muiden termien kanssa.

Tietyllä taajuusvaiheen arvolla tulokseksi saatiin pulssille yli kaksinkertainen huipputeho ja kaksi kertaa alhaisempi FWHM-arvo verrattuna tasavaiheiseen pulssiin. Optinen teho tietyillä aallonpituuksilla pystyttiin kaksinkertaistamaan tai vaihtoehtoisesti vähentämään lähes nollaan. Optisen tehon muutos tietyillä aallonpituuksilla huomattiin olevan eri suuruinen, riippuen tutkittavasta aallonpituusvälistä.

Avainsanat: superjatkumon generoiminen, split-step Fourierin menetelmä, spektrinen vaihe, yleistetty epälineaarinen Schrödingerin yhtälö

Tämän julkaisun alkuperäisyys on tarkastettu Turnitin OriginalityCheck -ohjelmalla.

CONTENTS

1. Introduction	1
2. Theoretical background	3
2.1 Dispersion	3
2.2 Nonlinear optics	3
2.3 Third order susceptibility	4
2.3.1 The Kerr-effect	4
2.3.2 Self-phase modulation	5
2.3.3 Four-wave mixing	5
2.4 Raman scattering	6
2.5 Solitons	7
2.6 Generalized nonlinear Schrödinger equation	8
2.7 Supercontinuum	8
3. Numerical methods.	10
3.1 Split-step Fourier method	10
3.2 Optimization methods	11
3.2.1 Optimization of pulse compression	11
3.2.2 Optimization of wavelength targeting	13
4. Results	14
4.1 Setup	14
4.2 Pulse compression	15
4.3 Spectral control	18
4.4 Coherence properties	20
5. Summary.	24
References.	26

1. INTRODUCTION

Supercontinuum generation (SCG) is a process where the spectrum of a narrowband optical pulse is broadened significantly. This happens due to the vast nonlinear interactions experienced by the pulse in a nonlinear medium. Supercontinuum (SC) was first discovered in 1970, by R. R. Alfano and R. S. Shapiro, who were studying self-phase modulation (SPM) with narrowband pulses [1, 2]. Alfano and Shapiro referred to the findings originally as "the ultimate white light source", but due to the extreme, and at the time vaguely understood, broadening of the spectrum, the name supercontinuum was asserted in the 1980s. SCG research peaked in popularity for the first time in 1992 when possible applications to telecommunications were first considered [3]. This, in combination with the progress in silica fibers facilitated rapid growth for the research.

The spectral broadening accompanied by the interesting coherence properties have continued to bring the field of SCG abundant attention regarding application possibilities in bio-imaging, laser sorting, device characterisation and others. More recent advancements in the fields of light sources and waveguides [4] have enabled SC research to achieve the extremely nonlinear conditions required in the process more efficiently. Increase in the computing power has also improved the possibilities of numerical study of SCs.

Since SCG is governed by complex linear and nonlinear interactions, its purely theoretical study is extremely tedious and in some cases impossible. To overcome this difficulty, one can implement a numerical method as an alternative solving method. Using a numerical method not only facilitates the theoretical analysis but also brings a more versatile method as opposed to laboratory testing. There have been a few studies on supercontinuum response to phase modification [5, 6, 7], but so far they have mainly focused on intensity splitting, delaying and recombining of the wavefronts. Only Schenkel et al. [6] have had the same approach of modifying the input pulse phase, than us. However their study was limited to a propagation length of 5mm, which resulted in a supercontinuum much narrower than what can be achieved now. Shifting power between specific wavelengths on the spectrum has also been shown to be possible by controlling the spectral phase of the input pulse in [8].

The purpose of this thesis is to introduce a numerical method for inspecting the properties of supercontinuum with spectral phase modulation. The numerical method is used to examine the effects of spectral phase modulation on the pulse compression capabilities, as well as on the targeting of individual wavelengths. Lastly the coherence properties of supercontinuum pulse trains are studied. This thesis is then organised as follows: Chapter 2 gives a brief introduction to the generalized nonlinear Schrödinger equation (GNLSE) governing the pulse evolution in the medium and the most important nonlinear interactions described by it. In addition some properties of supercontinuum are discussed in more detail. Chapter 3 is focused on explaining the numerical aspects of the study including the Split-step Fourier method, which is used to model the pulse propagation and the general optimization method used for finding the desired phase components. The results and summary are presented respectively in Chapters 4 and 5.

2. THEORETICAL BACKGROUND

2.1 Dispersion

Material dispersion is an optical phenomenon which states that the phase velocity of light in a material is proportional to its frequency [9]. This can be understood as the refractive index of the material being a function of frequency. All materials possess unique dispersion properties.

The material dispersion $\beta(\omega)$ is generally expanded into its Taylor series as

$$\beta(\omega) = \beta_0 + \beta_1(\omega - \omega_0) + \frac{1}{2}\beta_2(\omega - \omega_0)^2 + \dots, \quad (2.1)$$

where ω_0 is the central frequency. Of special interest to us is the second order term β_2 which is also referred to as the group velocity dispersion (GVD). Using the GVD parameter β_2 , material dispersion can be classified as either normal or anomalous. Normal dispersion is observed when $\beta_2 > 0$ is satisfied. In other words, normal dispersion occurs when the refractive index increases concurrently with the present frequency. Anomalous dispersion is the opposite; the refractive index decreases with increasing frequencies and thus $\beta_2 < 0$ is satisfied. [10]

2.2 Nonlinear optics

Understanding the concept of a nonlinear process is important when examining SCG, since a cascade of such operations are present in it. If a process fulfills the condition

$$f(ax_1 + bx_2) = af(x_1) + bf(x_2), \quad (2.2)$$

where a and b are constants and x_1 and x_2 are independent input values for the function $f(x)$, it is considered linear. If 2.2 is not fulfilled, the process is nonlinear. In theory this condition is fulfilled by a multitude of physical processes, but in the real world, every process has some amount of nonlinearity. However, when these nonlinearities are insignificant compared to the dominant effects, the process can be treated as linear [11].

Nonlinear optics is the study of nonlinear responses of a dielectric material to an intense electric field. These responses can be quantified with the materials polarization. The response of polarization $P(t)$ to an electric field $E(t)$ can be written as

$$P = \epsilon_0(\chi^{(1)}E(t) + \chi^{(2)}E^2(t) + \chi^{(3)}E^3(t) + \dots), \quad (2.3)$$

where $\chi^{(n)}$ represents the n:th order susceptibility and ϵ_0 is the permittivity of vacuum [12]. Both $P(t)$ and $E(t)$ are functions of time. The only susceptibility term appearing in a linear situation is the first order term $\chi^{(1)}$ and it can be related to the relative permittivity ϵ_R , and thus the refractive index n by

$$n^2 = \epsilon_R = 1 + \chi^{(1)}. \quad (2.4)$$

The higher order terms, especially $\chi^{(3)}$, give rise to nonlinear effects, of which some of the most important ones to our case are discussed in more detail below.

2.3 Third order susceptibility

In the following sections some of the processes arising from the third order susceptibility $\chi^{(3)}$ seen in equation 2.3 are introduced. These processes occur in all materials to some degree, but play a major role in supercontinuum generation in the form of creating new frequency components to the electric field. Also, as will be shown in following sections, the third order susceptibility interactions can be self-induced and are proportional quadratically to the input electric field.

2.3.1 The Kerr-effect

The Kerr effect can be described as the change in the materials refractive index in relation to an external electric field. The Kerr effect can be divided into two different variations: AC Kerr-effect and DC Kerr-effect. DC Kerr-effect is a consequence of an outer independent electric field, and thus it can be observed with low-intensity light pulses when the external electric field is sufficiently more powerful. The AC Kerr-effect in turn arises from the pulses own electric field and therefore it can only be detected with highly intense light pulses. The latter is also referred to as the optical Kerr-effect and it is the more relevant of the two regarding supercontinuum generation. The change in the refractive index is proportional to the third order susceptibility term seen in eq. 2.3 and consequently quadratically proportional to the electric field of the pulse ($\propto E^2(t)$). The refractive index dependence can be written as

$$\Delta n = n_2 I(t), \quad (2.5)$$

where $I(t)$ is the intensity of the pulse and n_2 is the second order refractive index which is proportional to the mentioned third order susceptibility term [12]. Note that 2.5 does not represent the refractive index, but the difference between the value of the refractive index with and without the impinging electric field. The refractive index including the optical Kerr-effect can now be written as

$$n = n_0 + n_2 I(t), \quad (2.6)$$

where n_0 is the linear part of the refractive index. This representation of the optical Kerr-effect is however an approximation and it deviates slightly in the presence of ultrashort pulses with very wide spectra in the form of an effect called self-steepening. Self-steepening causes variations in the temporal shape of the pulse and can lead to a shock-effect, where the pulse essentially collapses on itself [13].

2.3.2 Self-phase modulation

Another phenomenon induced by the optical Kerr-effect is called self-phase modulation (SPM). It results from the varying refractive index, which induces variations called chirps into the pulses temporal phase [14]. The various spectral components have now a time dependence which, when linear, is either positive or negative. Positive chirp signifies a positive time dependence of the instantaneous frequency i.e. $\delta\omega(t) = \frac{d}{dt}\phi_{NL} > 0$, where $\omega(t)$ is the instantaneous frequency and ϕ_{NL} the temporal phase, and negative chirp the opposite. These chirps can create new frequency components and thus contribute to SCG.

2.3.3 Four-wave mixing

Four-wave mixing (FWM) is also an effect arising from the third order susceptibility in which, as the name suggests, four individual waves are interacting. The interaction between these waves can produce waves with new frequency components or in another case amplify already existing frequency components within the waves.

Assume we have four waves with distinct frequencies $\omega_1, \omega_2, \omega_3$ and ω_4 with wavenumbers k_1, k_2, k_3 and k_4 respectively. Following the third order nonlinearities in the medium, we can observe the annihilation of two of these components ω_1, ω_2 and a creation of two new components ω_3 and ω_4 . In order for this process to happen the energy must be conserved. Also contrarily to SPM, FWM is a phase-sensitive process, which means

that all of the waves must be in phase and thus momentum must be conserved. These conditions can be written respectively as

$$\omega_1 + \omega_2 = \omega_3 + \omega_4 \quad (2.7)$$

and

$$k_1 + k_2 = k_3 + k_4. \quad (2.8)$$

It is also common for other variations of frequency generation to occur where a single new frequency component is generated from three individual fields. This can happen via sum-frequency generation (SFG) where the frequency of the invoked field is a sum of three interacting fields, i.e. $\omega_4 = \omega_1 + \omega_2 + \omega_3$. Difference-frequency generation (DFG) is referred to when $\omega_4 = \omega_1 + \omega_2 - \omega_3$ occurs. An energy level diagram of FWM is illustrated in figure 2.1.

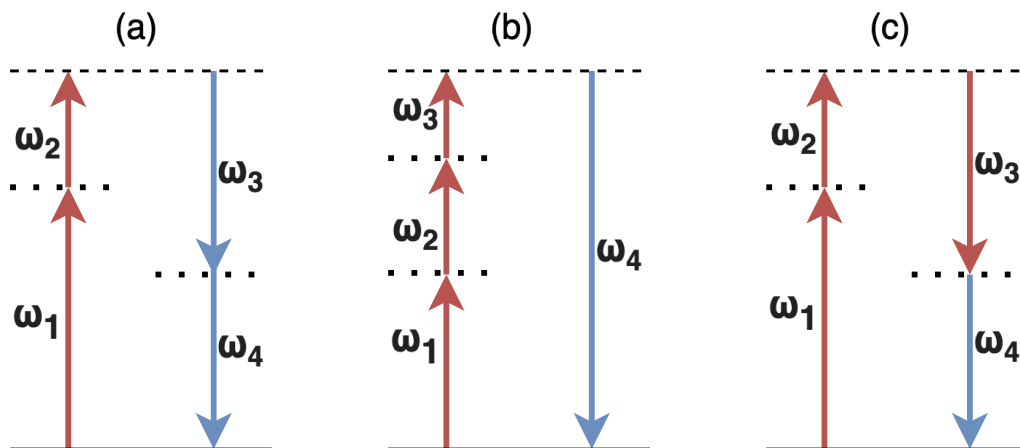


Figure 2.1. Energy level diagrams for various nonlinear processes. (a) Four-Wave Mixing (FWM); (b) Sum Frequency Generation (SFG); (c) Difference Frequency Generation (DFG). Red energy transitions represent initially present and blue newly generated frequency components.

2.4 Raman scattering

Raman scattering (RS) is a phenomenon characteristic for high power pulses in molecular mediums where a small fraction of arriving optical fields energy is transferred to another field or vice versa. It is the result of inelastic scattering of light in material. When the optical incident field loses energy to the molecular lattice, following its frequency to be shifted downwards, the process is called Stoke scattering. Contrarily when a photon meets a molecule with an already excited vibrational state, it can scatter by absorbing the excess

energy in a process called anti-Stokes scattering. [12]

As the magnitude and sign of RS are dependent on the vibrational modes present in the medium, different materials exhibit different forms of it. RS can be tailored to achieve gain for specific frequency components with the choice of materials. For example, Raman gain in silica fibers can be extended to frequency ranges of up to 20 THz [15].

Spontaneously occurring Raman scattering is a weak process which transfers approximately 10^{-6} of the incident optical field power to other fields, but with extreme powers and nonlinear medium one can excite stimulated Raman scattering (SRS), of which the transfer of energy can be up to 10% [12]. SRS is a prominent effect in supercontinuum generation.

2.5 Solitons

In a special occurrence, the dispersive and nonlinear effects of the nonlinear medium can cancel one another out. This situation forms an equilibrium between the pulse broadening and pulse compressing and results in a wave packet referred to as a soliton. Solitons can travel significant distances unchanged in a medium even in the event of a collision with another soliton. In anomalous dispersion regime solitons are formed when the spectral broadening induced by the GVD is countered by the SPM induced phase shift.

From a mathematical viewpoint solitons are solutions of the GNLSE and they generally have the shape of a hyperbolic secant pulse ($sech^2(t)$). A soliton described earlier is a first order soliton ($N=1$) and it is referred to as a fundamental soliton. Higher order solitons ($N>1$) are also possible. Unlike fundamental solitons, the pulse shape of a higher order soliton is not constant during propagation, but rather it oscillates periodically, returning into its original shape after one soliton period. The soliton order number N describing the order of a given soliton can be expressed as

$$N^2 = \frac{\gamma P_0 T_0^2}{|\beta_2|}, \quad (2.9)$$

where P_0 is the peak power of the pulse, T_0 is the width of the pulse measured in $T_{FWHM}/1.763$, β_2 is the GVD parameter and γ is the nonlinear coefficient [16]. The numerical factor in $T_0 = T_{FWHM}/1.763$ allows the width of the pulse to be given in FWHM.

Higher order solitons can achieve effective pulse compression but are in some cases difficult to sustain due to their tendency to shatter into fundamental solitons and disper-

sive waves. The splitting of such higher order solitons is called soliton fission and it can in turn lead to supercontinuum generation [17].

2.6 Generalized nonlinear Schrödinger equation

Supercontinuum generation in nonlinear fibers is governed by the generalized nonlinear Schrödinger equation. The GNLSE expresses quantitatively how the previously mentioned effects act on a pulse, when it is propagating in a nonlinear fiber. It can be written as

$$\frac{\partial A(z; T)}{\partial z} + \frac{\alpha}{2} A(z; T) - \sum_{k \geq 2} \frac{i^{k+1}}{k!} \beta_k \frac{\partial^k A(z; T)}{\partial T^k} = i\gamma \left(1 + i\tau_{shock} \frac{\partial}{\partial T} \right) A(z; T) |A(z; T)|^2, \quad (2.10)$$

where z is the propagation direction, along the length of the fibre, $T = t - \beta_1 z$ is the co-moving time, indicating that we are following the dynamics of a pulse moving with group velocity β_1 and α accounts for the losses. β_k Represents the various dispersion orders which are fixed by the material, γ is the nonlinear coefficient, and τ_{shock} is the shock factor [16]. Moreover, the left-hand-side of the equation above contains the linear dynamics of the pulse propagating in the fibre, while the nonlinear dynamics, namely Kerr effect and shock dynamics, are represented by the first and second term on the right-hand-side, respectively.

2.7 Supercontinuum

We have now introduced some of the most prominent nonlinear effects to our case as well as the equation which dictates the pulse response to these effects. Next we give a brief introduction to supercontinua. Supercontinuum generation is a process where the spectral profile of a pulse is broadened to extreme bandwidths. The generated spectrum is also commonly flat in a sense that the spectral power is distributed smoothly around the central frequency. SCG is a consequence of the various nonlinear effects discussed above in combination with dispersion. An arbitrary SCG process is illustrated in 2.2.

The SCG mechanism is different depending on the duration of the input pulse. With long pulse durations ($\gtrsim 500$ fs), the supercontinua arise mainly from background noise amplified by SRS and FWM [18]. Other nonlinear effects can also be triggered when phase-matching conditions are met.

A more relevant situation for our case is the SCG with short and ultrashort pulses. Con-

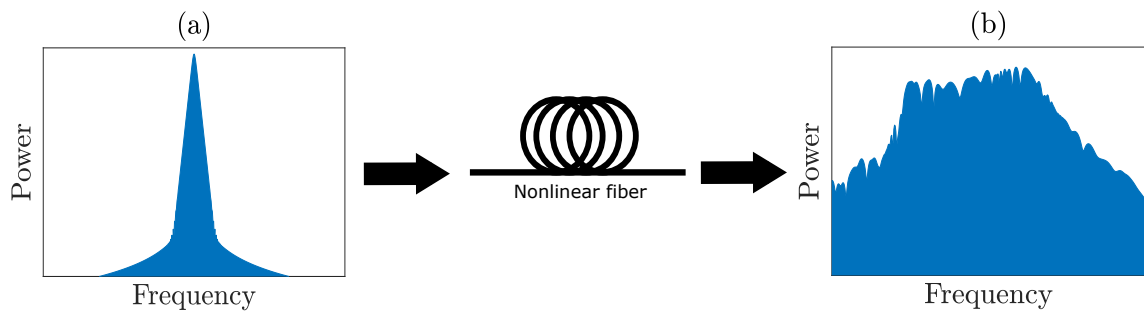


Figure 2.2. Pictorial representation of the SCG process. An input pulse with a narrow frequency spectrum (a) is let to propagate in a nonlinear fiber, resulting in a widened spectrum (b).

trarily to the case of long pulses, short pulse supercontinua are generated mainly from the incident field frequency components via $\chi^{(3)}$ -related effects such as SPM. In normal dispersion regime, the main contributors to SCG are SPM and FWM [19]. In this regime, the interaction length is usually kept short because the nonlinear effects take place early in the fiber, and a longer propagation distance only allows the dispersion of the fiber to broaden the pulse in temporal domain and therefore narrow the spectrum.

Generally in anomalous dispersion region, SPM acts together with dispersion and gives rise to complicated soliton mechanics. Such mechanics are readily available since a commonly used input pulse shape $\text{sech}^2(t)$ is a high order soliton itself. Soliton fission is the main SCG effect in the anomalous regime. Compared to the normal dispersion regime, supercontinuum generated in the anomalous regime have a less "flat" spectral profile [20] and usually poor temporal coherence properties [21].

In addition to the effects that are mostly defined by the properties of the waveguide, SG is highly dependent on the peak power, duration, pump frequency and, as we will find out in later chapters, the phase of the input pulse.

3. NUMERICAL METHODS

3.1 Split-step Fourier method

As mentioned, the GNLSE can be tedious to solve analytically. To overcome this difficulty, a numerical method is generally implemented. A common approach in the case of single mode fibers, is to use the Split-Step Fourier Method (SSFM) [22]. The SSFM is a pseudo-spectral method and it approaches the problem by separating the equation into smaller parts, which can be by themselves solved analytically. The SSFM functions as follows: first, we separate the linear part of the GNLSE

$$\frac{\partial A(z; T)_L}{\partial z} = \left(-\frac{\alpha}{2} + \sum_{k \geq 2} \frac{i^{k+1}}{k!} \beta_k \frac{\partial^k}{\partial T^k} \right) A(z; T) = \mathcal{L}A(z; T), \quad (3.1)$$

where the losses and the various dispersion terms are summarised in the linear operator as \mathcal{L} . The remaining part of the equation represents the nonlinear response of the fiber and it is in the form of

$$\frac{\partial A(z; T)_N}{\partial z} = i\gamma \left(1 + i\tau_{shock} \frac{\partial}{\partial T} \right) |A(z; T)|^2 A(z; T) = \mathcal{N}A(z; T), \quad (3.2)$$

where now the nonlinear response is summarised by the nonlinear operator \mathcal{N} . With these definitions at hand, the GNLSE can be then written in the following form, which is convenient for numerical implementation:

$$\frac{\partial A(z; T)}{\partial z} = (\mathcal{L} + \mathcal{N}) A(z; T). \quad (3.3)$$

We can now get an approximation of the whole function by propagating the linear part and the nonlinear part alternately in short steps. The nonlinear step is performed in time domain and it takes the form

$$A(z + h; T)_N = \exp(\mathcal{N}h)A(z; T)_N, \quad (3.4)$$

where h is the length of the step taken. The linear part of the equation is analytically solvable only in the frequency domain and therefore a Fourier transform of the pulse must

be taken before the linear step is carried on. The complete solution after a propagation step h can be then written as

$$A(z + h, T) = \mathcal{F}^{-1} (\exp(\mathcal{L}h) \mathcal{F} (\exp(\mathcal{N}h) A(z, T))), \quad (3.5)$$

where \mathcal{F} denotes Fourier transformation with respect to the temporal variable T , and \mathcal{F}^{-1} is the inverse Fourier transform. The approximation approaches the analytical solution when the step size h is infinitesimal, but because each additional step requires more computational power, a finite value is used for calculations. Selecting an appropriate step size requires careful consideration of the involved linear and nonlinear effects. When the step size is chosen sufficiently, the approximation remains valid.

3.2 Optimization methods

The solution space of GNLSE is essentially infinite due to the co-evolving temporal and spectral phases as well as the nonlinearities present. This results in a very difficult process of finding the desired solutions, and it is sometimes approached with genetic algorithms and machine learning. An alternative approach that requires less computing power and can be implemented with a simpler algorithm, is to decrease the parameter space. This can be done by expanding the spectral phase to an Taylor series

$$\begin{aligned} \varphi(\omega) = & c_0 \varphi_0 + c_1 \varphi_1 (\omega - \omega_0) \\ & + c_2 \varphi_2 (\omega - \omega_0)^2 + c_3 \varphi_3 (\omega - \omega_0)^3 + \dots, \end{aligned} \quad (3.6)$$

where c_n is the relative weight on the n :th order phase component, φ_n the n :th order coefficient given by the Taylor expansion and ω_0 a reference frequency chosen to be as the center frequency for the input spectrum. With this approach, the problem reduces from finding a solution in virtually infinite solution space to optimization of shown coefficients c_n .

3.2.1 Optimization of pulse compression

The optimization in our case was done in loops. The general idea of the optimization method was to find the highest possible peak intensity for the pulse since as the overall energy of the pulse is conserved, a higher intensity peak then means a shorter pulse duration. In an individual simulation, a single phase component was given some non-zero weight, and the pulse was propagated through the photonic crystal fiber (PCF). This procedure was done with a wide variety of different values for the component weight, and

the pulses with these phase values were formed on to a map. An example of this formed map is shown in figure 3.1.

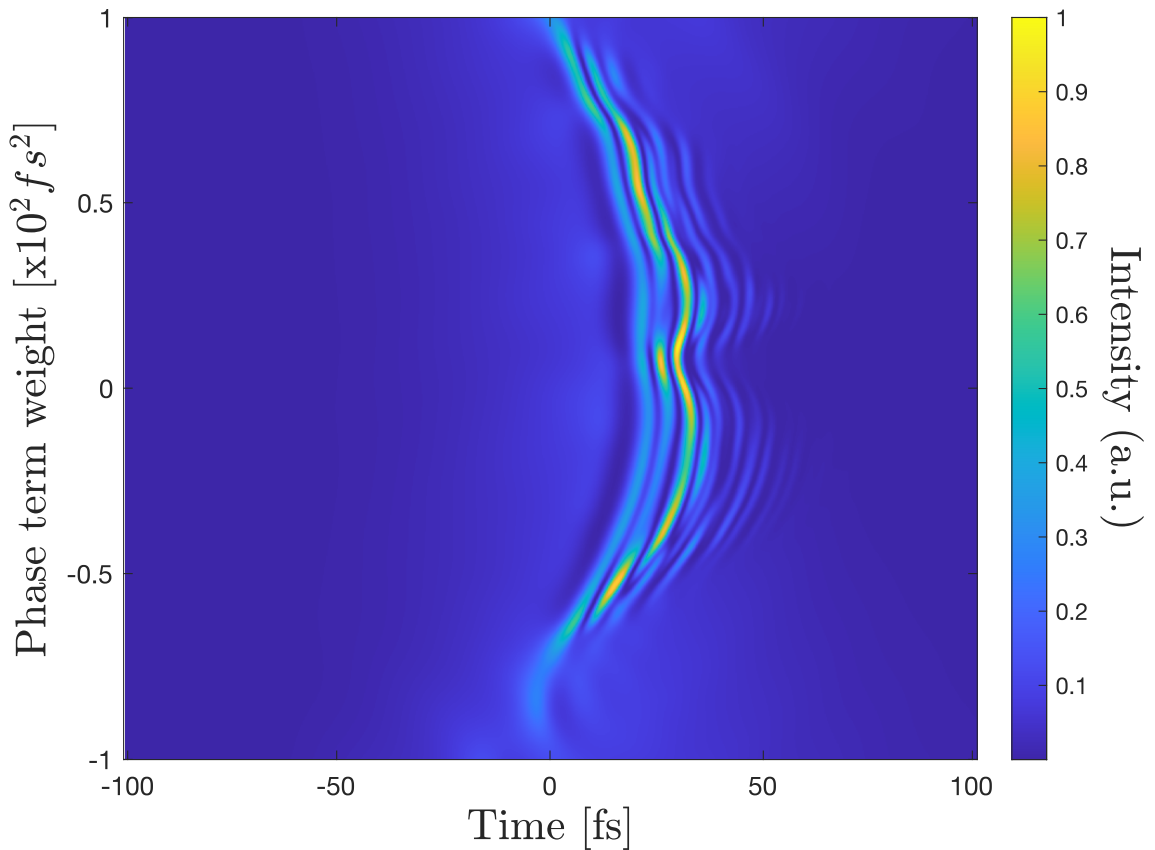


Figure 3.1. Example of a map showing the pulse shape after propagation when a phase weight is applied to the input pulse. Each row represents an individual pulse envelope corresponding to the weight specified in y-axis.

The x-axis in 3.1 represents the time in the moving frame of the pulse and y-axis the spectral phase component weight. These figures can be understood as multiple pulse envelopes lying horizontally, each corresponding to a given relative phase weight and they must not be confused with figures depicting pulse evolution which might appear similar. For clarity, A pulse envelope with no weight given on the phase component situates horizontally on $y = 0$.

From these maps, the component weights corresponding to the highest peak intensities were used for iterations with other phase components, meaning that when a desired value for one term is found, it is locked in place and a new map is formed by varying a different order term weight. After a value was found for each term, the loop was repeated to ensure converging into a value inside the parameter space.

3.2.2 Optimization of wavelength targeting

The method for increasing or decreasing the power carried by a specific wavelength followed a similar structure. Only now the map formed from varying an individual phase component is used to find the area of a small segment located under the desired wavelength. Similarly to figure 3.1, figure 3.2 illustrates the mapped values of one varied spectral phase component, only now the pulses are shown in wavelength-domain.

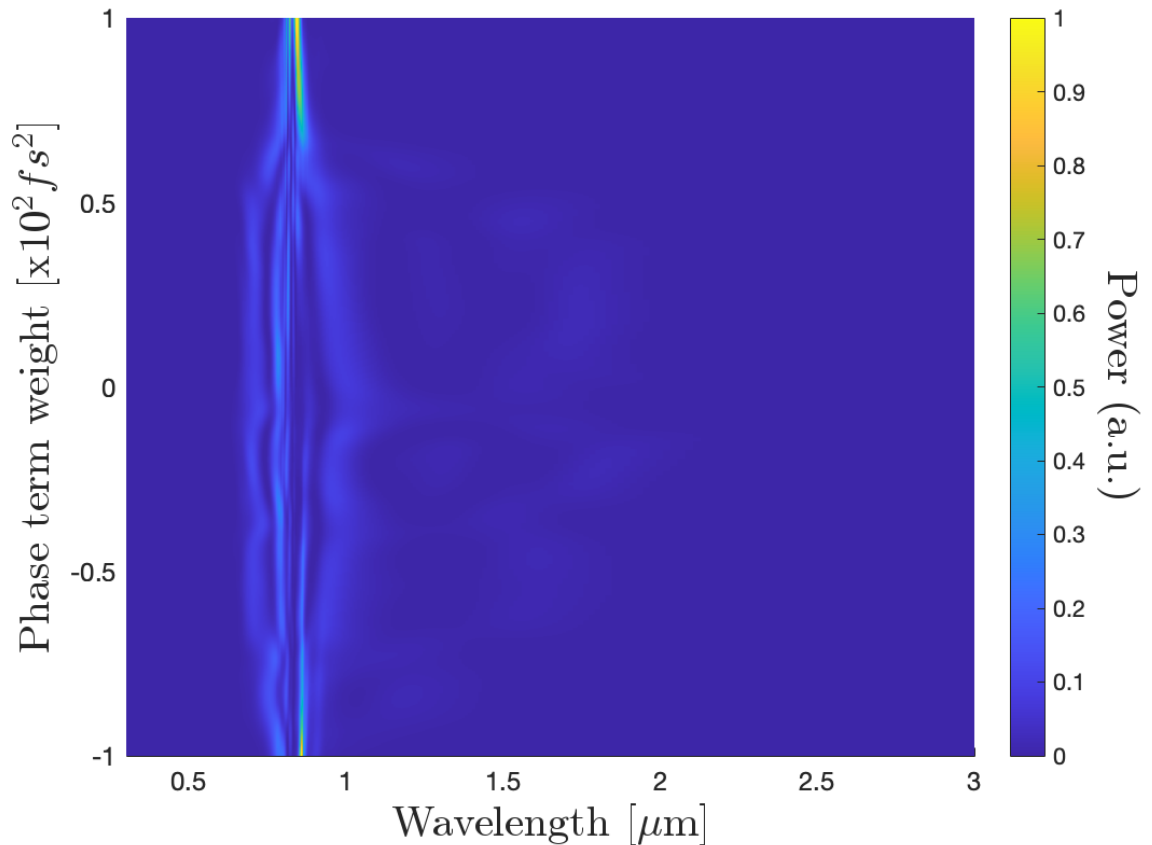


Figure 3.2. Example of a map similar to figure 3.1, only now in the wavelength domain

The y-axis on figure 3.2 represents again the relative weight of the phase component while the x-axis is for displaying the wavelengths in which the spectral power is distributed. The figure can now be understood similarly to figure 3.1, only now a single row depicts a spectral profile of a certain pulse.

4. RESULTS

4.1 Setup

The aforementioned split-step Fourier method is used for solving the GNLSE, and the optimization followed methods described in 3.2. The SSFM is suitable for our purposes because we are simulating a fiber which essentially supports only one single mode and therefore reduces the problem to one dimension. The propagating input pulse was in the form of a simple hyperbolic secant pulse

$$A(z; T) = \sqrt{P_0} \operatorname{sech}(1.7627 T/\tau), \quad (4.1)$$

where P_0 is the peak power of the pulse and τ the full width at half maximum (FWHM) of the pulse. The numerical factor inside the sech-pulse allows the width to be given in FWHM. The various spectral phase values were introduced by first Fourier transforming the pulse into the frequency domain and then adding the phase.

In these experiments the pulses were propagated through a 10mm long optical fiber in the anomalous dispersion regime, where the various dispersion parameters were the same ones that are used in [23] and are shown in table 4.1.

The peak power of the pulse was kept at 10kW and the pulse located around the center

$\beta_2 = -11.830 \text{ ps}^2/\text{km}$
$\beta_3 = 8.1038 * 10^{-2} \text{ ps}^3/\text{km}$
$\beta_4 = -9.5205 * 10^{-5} \text{ ps}^4/\text{km}$
$\beta_5 = 2.0737 * 10^{-7} \text{ ps}^5/\text{km}$
$\beta_6 = -5.3943 * 10^{-10} \text{ ps}^6/\text{km}$
$\beta_7 = 1.3486 * 10^{-12} \text{ ps}^7/\text{km}$
$\beta_8 = -2.5495 * 10^{-15} \text{ ps}^8/\text{km}$
$\beta_9 = 3.0524 * 10^{-18} \text{ ps}^9/\text{km}$
$\beta_{10} = -1.7140 * 10^{-21} \text{ ps}^{10}/\text{km}$

Table 4.1. Dispersion terms used in the simulations

wavelength of 835nm. The width of the input pulse was kept at a FWHM of 50fs.

4.2 Pulse compression

Firstly we studied the overall effects of varying the phase components on the temporal pulse shape and spectral profile of the output pulse. On figure 4.1 we have mapped the effects of the second and third order phase terms in a way mentioned in chapter 3.2.

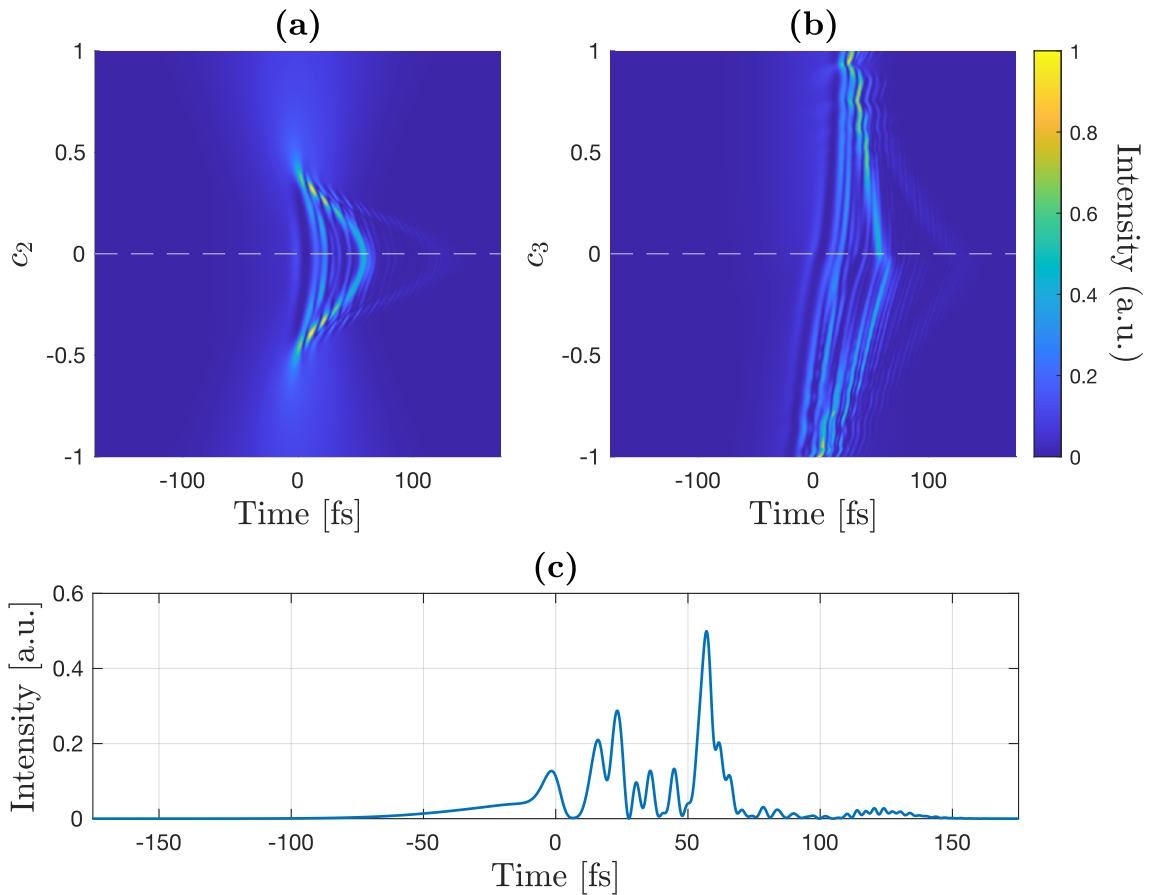


Figure 4.1. Maps of temporal pulse shapes corresponding to the varying of the second order (a) and third order (b) phase terms. The intensity scale is normalized. Panel (c) represents the pulse envelope with no phase modification, which is marked in (a) and (b) with a horizontal, white dashed line

The centermost row in both figures 4.1(a) and 4.1(b) correspond to the situation where the input pulse is endowed with a flat phase $c_n = 0$ and is therefore the same in both figures [see figure 4.1(c)]. One thing to note is the seemingly symmetrical appearance of fig 4.1(a) with respect to $c_2 = 0$. This symmetry is not apparent in fig 4.1(b), where negative term weights seem to shape the pulse dissimilarly compared to positive weights. The symmetrical behaviour was apparent with all even order terms up to the 8th term, where the effects were already difficult to notice, while the asymmetry in fig 4.1(b) could be seen in all of the odd order terms up to the 7th term. This symmetry would be expected in a linear situation, where only the dispersion shapes the phase, but is rather unexpected in

our nonlinear case.

The second and third order components were the major contributors on the increased peak intensity and thus the pulse compression. Some local maxima of intensities corresponding to the given c_2 weights are listed in table 4.2. Values mentioned in the table can easily be identified in fig 4.1(a) as the four greatest peaks.

c_2	I (kW)
0	25.574
-0.3907	51.203
-0.3364	50.425
0.3150	49.769
0.2594	46.201

Table 4.2. Relative phase weights c_2 with corresponding achieved peak intensities

As can be seen in 4.2, the peak intensity doubled when a specific value was inserted into just the second order phase component and the other terms were kept at zero. Certain third order component values also increased the peak intensity noticeably. With greater order components we notice a great decrease of influence in the peak intensity with the 8th and 9th order components having close to non-existent effects on the pulse shape. This behaviour is expected as the n :th term of a Taylor expansion is proportional to $1/n!$. The symmetrical tendencies of the second order component can also be seen from table 4.2 as the weights of the four greatest local maxima are found in similar distances from zero.

After the effects of individual phase components were studied and the values resulting in highest peak intensities were mapped we moved onto combining different phase terms. We firstly combined the individually found phase term weights that resulted in the highest increase in the peak intensity when applied alone and ran a simulation of the propagation. This method is however very unlikely to result in an optimally compressed pulse, since the various nonlinear effects provoke the co-evolving of the phase components. An optimization loop is required for this task. We began the optimization in most by locking in place a second order term weight corresponding to an earlier discovered increased peak intensity, and then moving through the terms in order of magnitude. We can expect to find the best solutions by starting from the second term since it appeared to have the most influence on the pulse compression. In figure 4.2(a), we show the pulse compression optimization results accompanied by the Fourier-transform-limited pulses in fig 4.2(b). Fourier-transform-limited pulse is defined as the pulse with the shortest temporal width corresponding to its spectral bandwidth. This is achieved when all the spectral components have a null phase. However due to the phase modulating effects of super-

continuum generation, it can only be achieved theoretically. The pulses are offset in time for clarity.

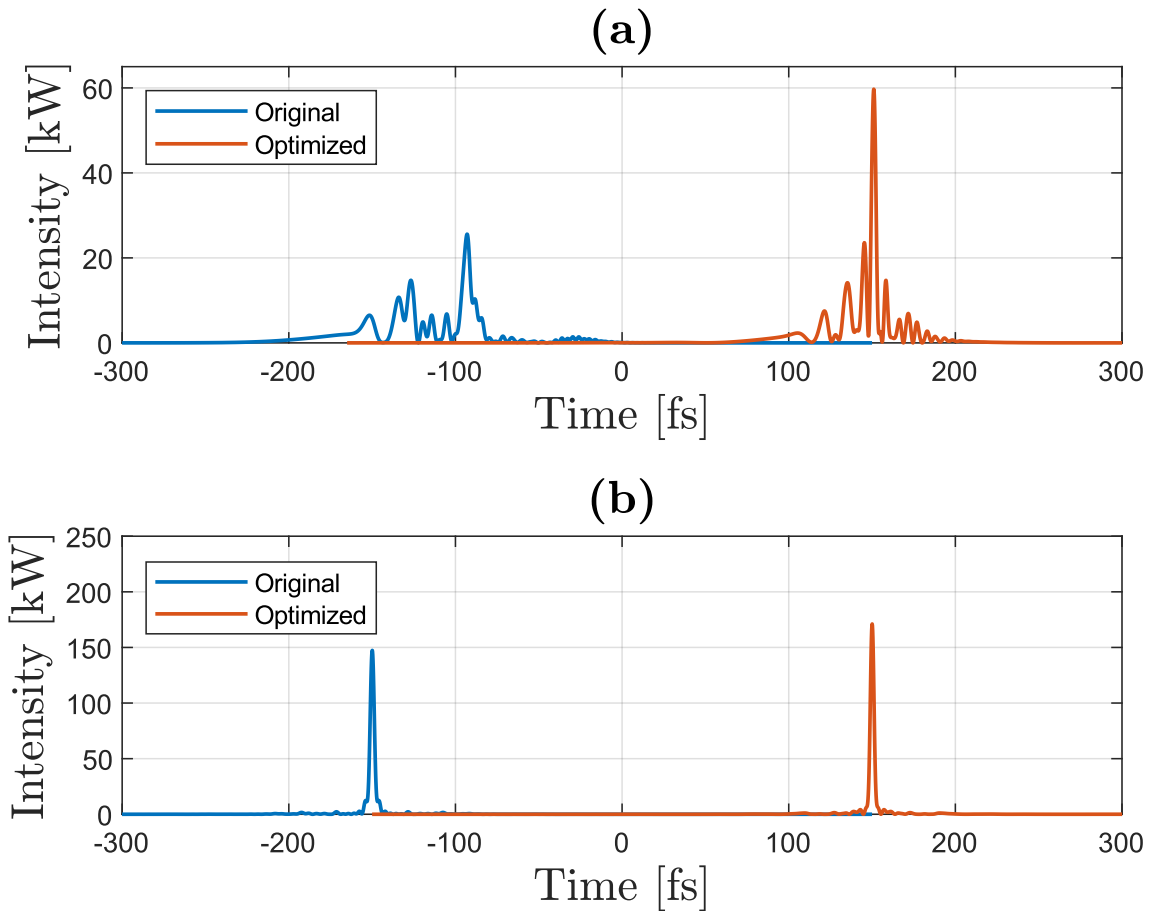


Figure 4.2. Comparison of the original and the optimized pulses with regard to pulse compression in (a). Fourier transform-limited pulses corresponding to each situation below in (b). Pulses are offset in time for clarity

In Figure 4.2(a) an output pulse resulting from a flat phased input pulse is shown on the left marked in blue, and a corresponding transform-limited pulse similarly on figure 4.2(b). We can see that the flat spectral phase in the input pulse results in an unpredictable temporal pulse on the output pulse, and rather than one clear peak, the power is distributed along many separated peaks. By studying the spectral profile of this pulse, we can see that the spectrum is greatly widened, which is result to the various nonlinear effects generating new frequency components. However these frequency components are not travelling simultaneously in time and therefore the temporal shape of the pulse is as shown. We can counter this effect by applying the found phase into the input pulse. An output pulse resulting from this is depicted on figure 4.2(a) on the right and its transform-limited pulse is again shown similarly in (b). The peak intensity is more than doubled compared to the original pulse and the pulse shape clearly approaches the transform-limited case. From shown transform-limited pulses we can also note that the spectral bandwidth of the optimized pulse is greater than the one displayed by the original pulse, as the relation is

inverse in the temporal domain. Comparison of spectral profiles is shown in figure 4.3.

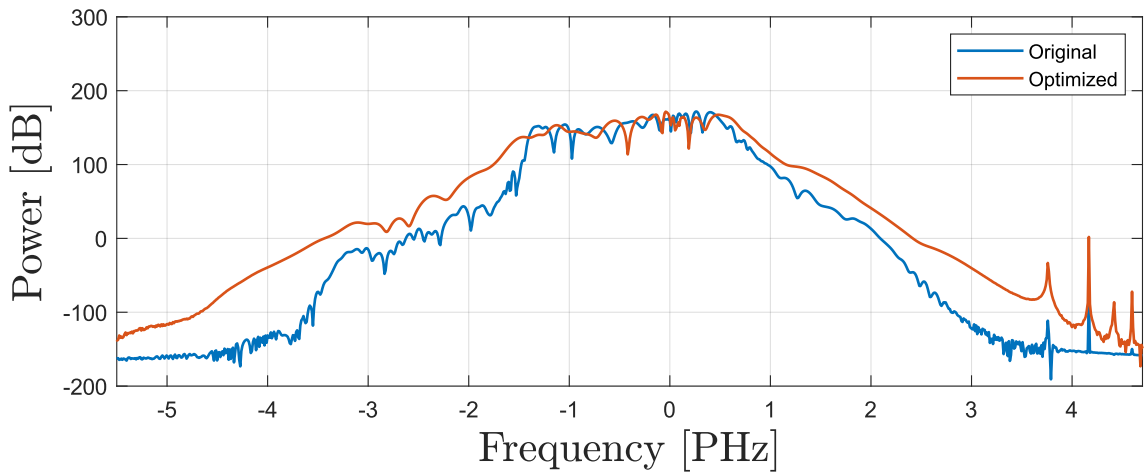


Figure 4.3. Power spectrum comparisons of the optimized and the original pulses in arbitrary units scaled in decibels.

The spectrum generated with the optimized phase is clearly wider as could be expected from inspecting figure 4.2. Note that the scale in figure 4.3 is in decibels.

4.3 Spectral control

Alongside pulse compression capabilities, we were also interested in how the phase modulation is able to transfer energy between specific frequencies of the pulse. This study followed a similar optimization method, compared to the former and thus we start by inspecting the overall effect of each phase term individually. This is shown again for the first two components in figure 4.4.

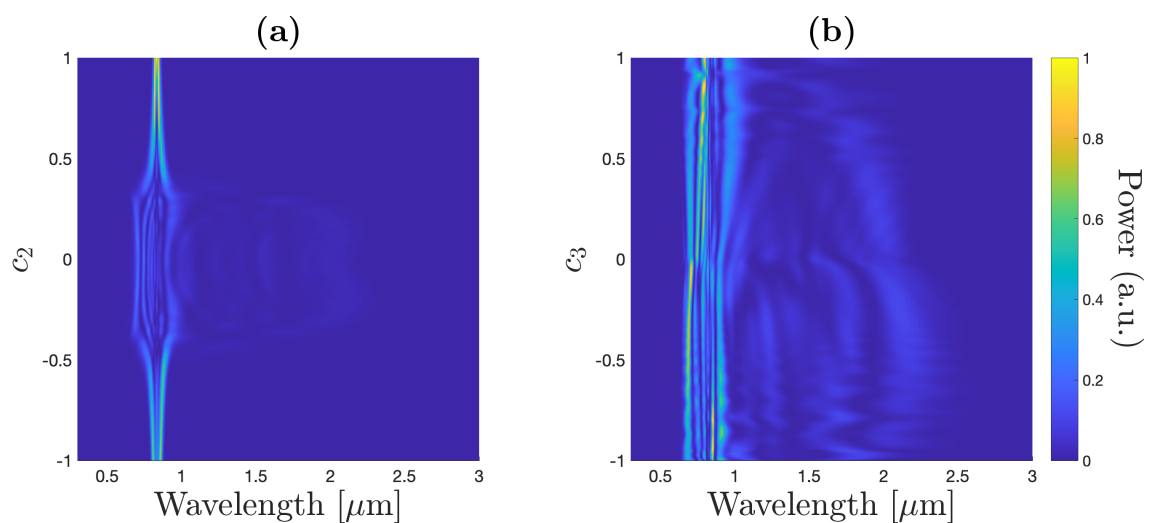


Figure 4.4. Shapes of spectral envelopes corresponding to the relative phase weight specified in y-axis. In (a) the second order term is varied and in (b) the third order. The power scale is normalized

Since figures 4.4(a) and (b) are fundamentally Fourier transforms of figures 4.1(a) and (b), we can notice all the same elements mentioned in the first part of chapter 4.2 in them.

We followed the study by combining the phase terms iteratively in a similar manner than earlier, but instead of pulse compression, our goal was to increase the power carried by chosen wavelengths. We performed this optimization individually to four different wavelengths in the range of 1000nm-2000nm and all of them resulted in an increase in the wavelength power. Results from optimizing the endpoints of our range are shown in figure 4.5.

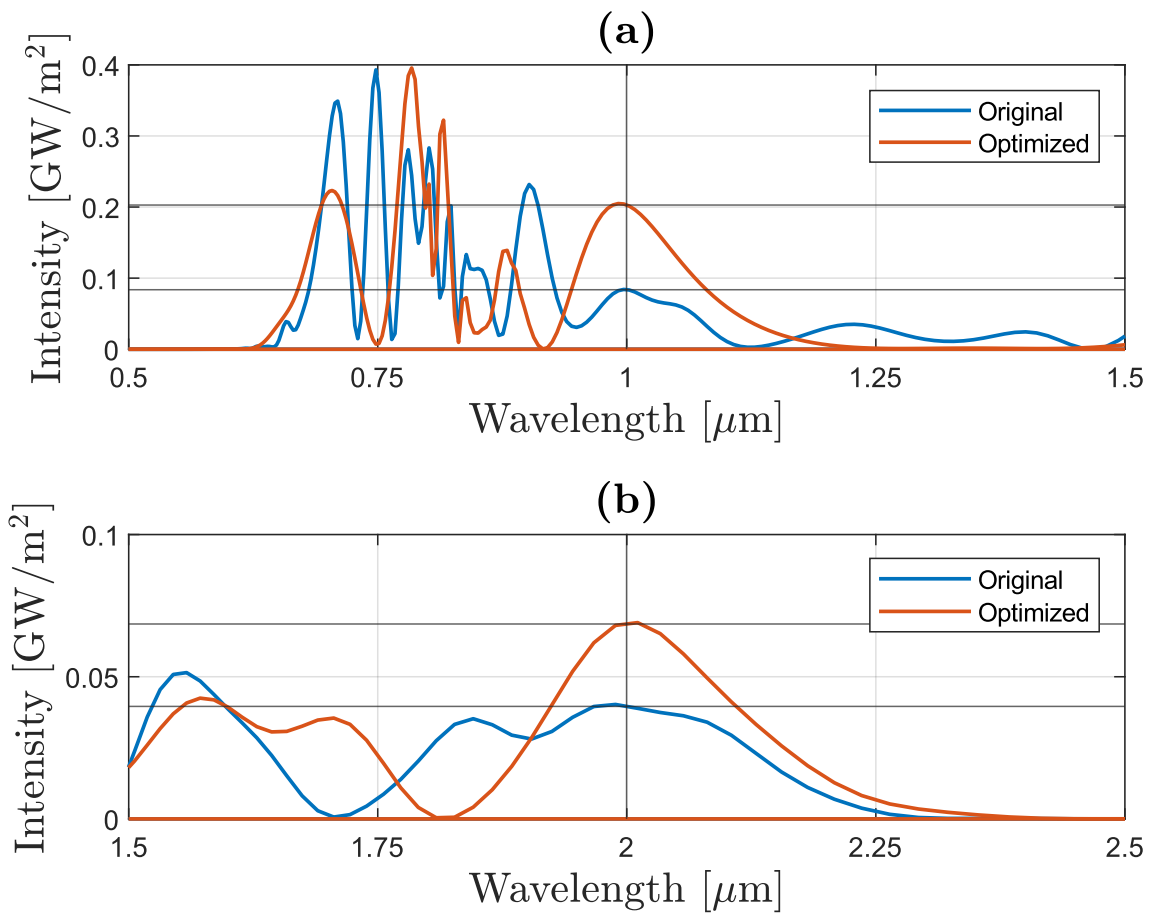


Figure 4.5. Comparisons of original and optimized spectral profiles with the aim of increasing the power carried by a specific wavelength. In (a) $\lambda = 1000nm$ is targeted and in (b) $\lambda = 2000nm$.

From the figure we can already note that the factor of which the power is increased by, is not constant. With some wavelengths the power could be doubled and with some the power was only 1.4 times of the power with a flat input phase. Due to the limited amount of simulations and the highly nonlinear nature of the interactions, a clear explanation for the difference in the power increase could not be given.

Additionally some trials were done to shift power away from chosen wavelengths. An

example of this, with the target wavelength $\lambda = 750\text{nm}$ is shown in figure 4.6.

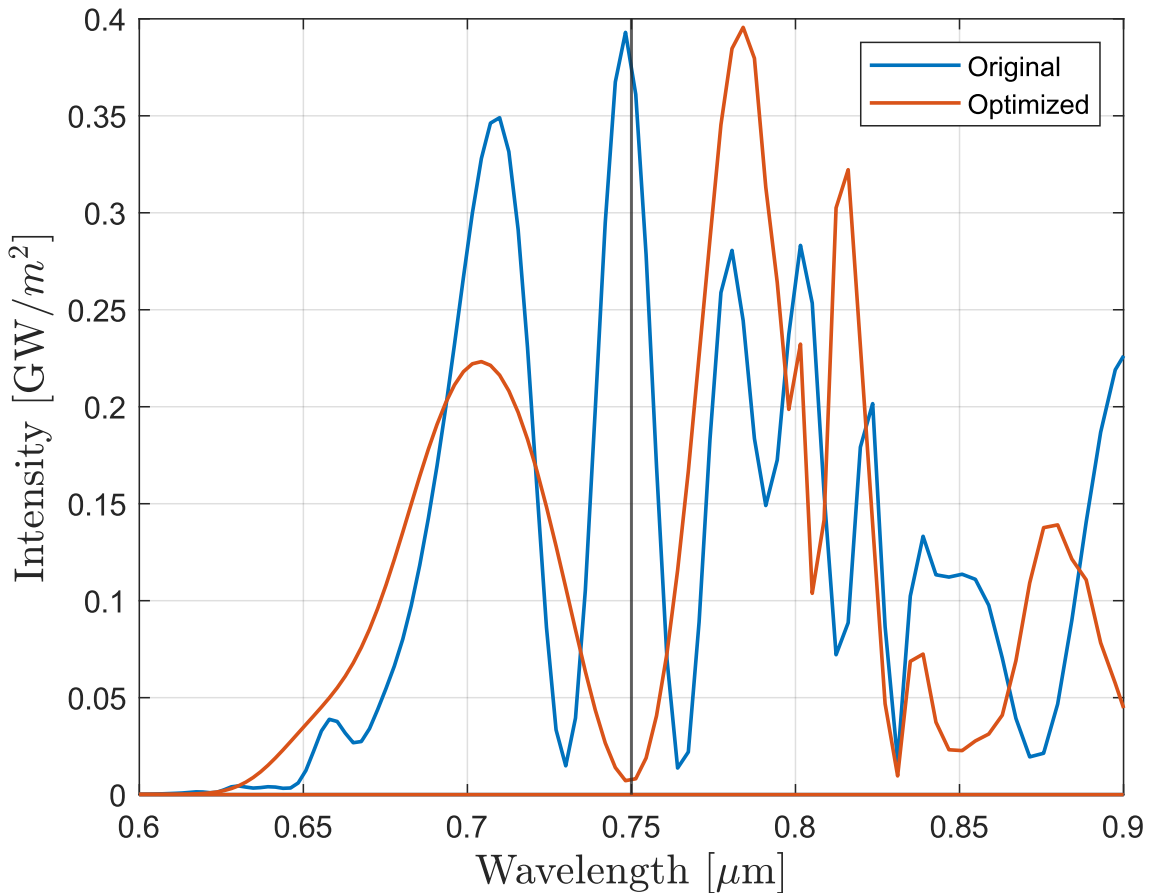


Figure 4.6. Spectral profiles of original and optimized pulses when power is shifted away from $\lambda = 750\text{nm}$.

Shifting power away from given wavelengths appeared to be more efficient than adding power to them. With right phase terms, the targeted wavelengths were able to be almost fully blanked. This is an interesting feature that could possibly pose a more flexible alternative to situations where Bragg gratings are used.

4.4 Coherence properties

Supercontinuum radiation can be used alongside optical instruments called frequency combs in which the spectral profile of the radiation is in the form of equidistant lines [24, 25]. These sort of spectral profiles can be formed with pulsed seed lasers where ultrashort pulses are formed with fixed pulse repetition rate, which in turn determine the inverse line spacing appearing on the spectral profile. This is result of spectral interference occurring on the overlapping spectral profiles provided by the subsequent pulses.

Measurements using a frequency comb usually require a spectrum with a broad overall bandwidth. One common method to achieve this is to use supercontinuum generation which can broaden the spectrum to span for over an octave. However the characteristics

of supercontinuum generation such as high input power, various nonlinear effects and the possible anomalous dispersion of the fiber contribute disruptively to the coherence of the pulse train and in many cases shape the individual spectral profiles unusable for interfering. Here we show how spectral phase modulation contributes to the coherence of discussed pulse trains in our case.

We can write the Mutual coherence function (MCF) as

$$\Gamma(t_1, t_2) = \frac{1}{N} \sum_n E_n^*(t_1) E_n(t_2) = \langle E^*(t_1) E(t_2) \rangle \quad (4.2)$$

where the angle brackets represent ensemble averaging, $E_n(t)$ is an individual realization from the pulse train and N is the amount of pulses present [26]. Fundamentally, the MCF depicts the pulses ability to interact with itself. Theoretical definition of MCF is when N approaches infinity, but for simplicity we compute with finite amount of pulses. With the help of MCF we can also introduce the concept of first degree of coherence $g^{(1)}$. It gives a quantitative measurement on the overall degree of coherence of the pulse train with $g^{(1)} = 1$ denoting perfectly coherent waves and $g^{(1)} = 0$ complete incoherence. MCF of pulse trains including 3, 1000 and 2000 pulses with modulated second order phase component are shown in figure 4.7.

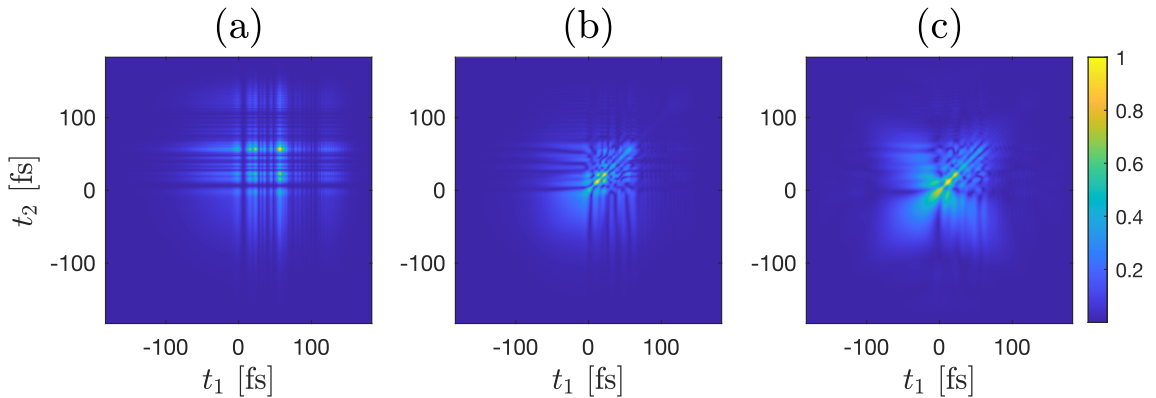


Figure 4.7. MCF of pulse trains with increasing amount of pulses and phase modulation in the second order term. Pulse amount in the train is 3 in (a), 1000 in (b) and 2000 in (c).

The distinguishable fringes in 4.7(a) indicate the potential of destructive and constructive interference which is a sign of high temporal coherence. This is expected since the train consists of only three pulses with a slight modification in the phases between them. Adding pulses to the train quickly decreases the coherence as is shown in figures 4.7(b) and 4.7(c).

In figure 4.8 we have applied the same treatment as in figure 4.7 to the varying of the third order phase component.

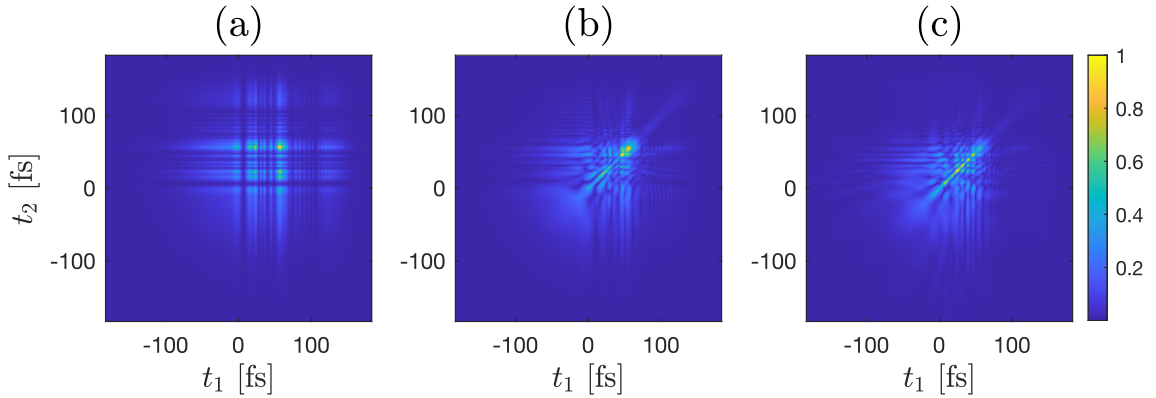


Figure 4.8. MCF of pulse trains with increasing amount of pulses and phase modulation in the third order term. Pulse amount in the train is 3 in (a), 1000 in (b) and 2000 in (c).

Again, the addition of pulses to the pulse train accounts for the loss of coherence. Figure 4.8(a) is intrinsically the same as figure 4.7(a), since only three pulses with very little phase modulation are in the train. However with higher number of pulses in the train, we can see the distinct behaviour of the third order phase component.

Compared to the second order phase term modulation, the loss of coherence was greater with the third order component. Values for these and other components before and after propagation are listed in table 4.3.

Phase term	$g^{(1)}$ before propagation	$g^{(1)}$ after propagation
c_2	0.9254	0.5219
c_3	0.9697	0.4021
c_4	0.9877	0.5290
c_5	0.9930	0.5046
c_6	0.9997	0.8887
c_7	0.9997	0.8480
c_8	1.0000	0.9773
c_9	1.0000	0.9935

Table 4.3. $g^{(1)}$ Values for pulse trains with 2000 realizations and phase modulation on a given phase term before and after propagation.

One might expect for the $g^{(1)}$ values to be opposite for the third and second order terms, since the second order term was found to have a bigger impact on the pulse than the third one, and generally more variance on the pulses leads to lesser coherence. However, as noted in chapter 4.2, the odd-order terms exhibit a sort of asymmetry with regard to the phase term weight, which might explain the coherence difference, since our pulse train consists of pulses with both positive and negative phase weights. The fact that the overall

degree of coherence was relatively lower with all odd-order terms in comparison to the even order terms strengthens this suggestion, but since we do not know the reason for the difference in the symmetry, it is difficult to verify it.

5. SUMMARY

In this thesis, we have theoretically covered supercontinuum generation and the most important effects giving rise to it, as well as studied supercontinuum optimization using a numerical method. We have obtained results from pulse compression, wavelength targeting and temporal coherence properties of the supercontinuum by modifying the spectral phase of the pulse. The results indicate the phase modification of the input pulse to be a promising method regarding supercontinuum optimization.

They, moreover, indicate that a specific combination of phase term weights on a Taylor expanded spectral phase result in a compressed pulse. This compression showed to be over two times that of a pulse with no phase modification. The attributions to the pulse compression originated mainly from the first two studied phase components, and were increasingly lesser with higher order terms. A difference between the even and odd order terms was found in a form of symmetrical behaviour. A symmetry on the pulse shape between negative and positive phase weight values was noticeable on even order terms, but nonexistent with odd order terms.

We have shown that phase modification on the input pulse can shift power between wavelengths on the output pulse. Targeted wavelengths experienced increase or alternatively decrease on the power carried by them, depending on the chosen phase component values. Power carried by an individual wavelength was able to be increased by a factor of up to 2, and in some cases the wavelength was able to be almost fully blanked. Increase on the carried power showed to be somehow dependent on the chosen wavelength. In addition, our results showed that phase modification leads to disturbance on the temporal coherence of pulses in a pulse train. The coherence loss appeared to be of higher magnitude with odd order terms.

We also showed that it is possible to reduce the essentially infinite solution space of these optimizations by inspecting the first 9 terms of the Taylor expansion of the spectral phase. Simulations using our method converged to local maxima in all of the cases. The optimization method could possibly be enhanced in the future with the use of machine learning and genetic algorithms.

Our results indicate the method we used to have potential regarding supercontinuum control, and that additional studies might be beneficial. Further investigations on the effects of input pulse intensity and the length of the fiber could be done, to get a more comprehensive understanding of the method. The highly nonlinear effects present in the fiber, which are dependent on the mentioned factors, suggest that varying them might result in substantially different solutions. Also, a potential follow-up for this study would be to study the wavelength spectrum control more thoroughly by targeting multiple wavelength simultaneously.

REFERENCES

- [1] Alfano, R. R. and Shapiro, S. L. Observation of Self-Phase Modulation and Small-Scale Filaments in Crystals and Glasses. *Phys. Rev. Lett.* 24 (11 Mar. 1970), pp. 592–594. DOI: 10.1103/PhysRevLett.24.592. URL: <https://link.aps.org/doi/10.1103/PhysRevLett.24.592>.
- [2] Alfano, R. R. and Shapiro, S. L. Emission in the Region 4000 to 7000 Å Via Four-Photon Coupling in Glass. *Phys. Rev. Lett.* 24 (11 Mar. 1970), pp. 584–587. DOI: 10.1103/PhysRevLett.24.584. URL: <https://link.aps.org/doi/10.1103/PhysRevLett.24.584>.
- [3] Ania-Castañón, J., Smirnov, S., Kobtsev, S. and Turitsyn, S. Supercontinuum in telecom applications. *Conference on Lasers and Electro-Optics*. Optica Publishing Group, 2017, AF1A.2. DOI: 10.1364/CLEO_AT.2017.AF1A.2. URL: https://opg.optica.org/abstract.cfm?URI=CLEO_AT-2017-AF1A.2.
- [4] Cerqueira, S. A. Recent progress and novel applications of photonic crystal fibers. *Reports on Progress in Physics* 73.2 (Jan. 2010), p. 024401. DOI: 10.1088/0034-4885/73/2/024401. URL: <https://dx.doi.org/10.1088/0034-4885/73/2/024401>.
- [5] Andresen, E. R., Dudley, J. M., Oron, D., Finot, C. and Rigneault, H. Transform-limited spectral compression by self-phase modulation of amplitude-shaped pulses with negative chirp. *Opt. Lett.* 36.5 (Mar. 2011), pp. 707–709. DOI: 10.1364/OL.36.000707. URL: <http://ol.osa.org/abstract.cfm?URI=ol-36-5-707>.
- [6] Schenkel, B., Paschotta, R. and Keller, U. Pulse compression with supercontinuum generation in microstructure fibers. *J. Opt. Soc. Am. B* 22.3 (Mar. 2005), pp. 687–693. DOI: 10.1364/JOSAB.22.000687. URL: <http://josab.osa.org/abstract.cfm?URI=josab-22-3-687>.
- [7] Austin, D. R., Bolger, J. A., Sterke, C. M. de, Eggleton, B. J. and Brown, T. G. Narrowband supercontinuum control using phase shaping. *Opt. Express* 14.26 (Dec. 2006), pp. 13142–13150. DOI: 10.1364/OE.14.013142. URL: <http://www.opticsexpress.org/abstract.cfm?URI=oe-14-26-13142>.
- [8] Yallapragada, V. J., Rigneault, H. and Oron, D. Spectrally narrow features in a supercontinuum generated by shaped pulse trains. *Opt. Express* 26.5 (Mar. 2018), pp. 5694–5700. DOI: 10.1364/OE.26.005694. URL: <https://opg.optica.org/oe/abstract.cfm?URI=oe-26-5-5694>.
- [9] Fowles, G. R. *Introduction to Modern Optics (2nd Edition)*. Dover Publications, 1975. ISBN: 978-0-486-65957-2. URL: <https://app.knovel.com/hotlink/>

toc/id:kpIMOE0001/introduction-modern-optics/introduction-modern-optics.

- [10] Paschotta, R. *Chromatic Dispersion*. RP Photonics Encyclopedia. Apr. 2005.
- [11] Powers, P. E. and Haus, J. W. *Fundamentals of nonlinear optics*. eng. Second edition. Boca Raton, FL: CRC Press, Taylor Francis Group, 2017 - 2017. ISBN: 1-315-11643-X.
- [12] Boyd, R. W. *Nonlinear Optics, Third Edition*. 3rd. USA: Academic Press, Inc., 2008. ISBN: 0123694701.
- [13] DeMartini, F., Townes, C. H., Gustafson, T. K. and Kelley, P. L. Self-Steepening of Light Pulses. *Phys. Rev.* 164 (2 Dec. 1967), pp. 312–323. DOI: 10.1103/PhysRev.164.312. URL: <https://link.aps.org/doi/10.1103/PhysRev.164.312>.
- [14] Stolen, R. H. and Lin, C. Self-phase-modulation in silica optical fibers. *Phys. Rev. A* 17 (4 Apr. 1978), pp. 1448–1453. DOI: 10.1103/PhysRevA.17.1448. URL: <https://link.aps.org/doi/10.1103/PhysRevA.17.1448>.
- [15] Mussot, A., Kudlinski, A., Habert, R., Dahman, I., Mélin, G., Galkovsky, L., Fleureau, A., Lempereur, S., Lago, L., Bigourd, D., Sylvestre, T., Lee, M. W. and Hugonnot, E. 20 THz-bandwidth continuous-wave fiber optical parametric amplifier operating at 1 μm using a dispersion-stabilized photonic crystal fiber. *Opt. Express* 20.27 (Dec. 2012), pp. 28906–28911. DOI: 10.1364/OE.20.028906. URL: <https://opg.optica.org/oe/abstract.cfm?URI=oe-20-27-28906>.
- [16] Agrawal, G. *Nonlinear fiber optics*. eng. Sixth edition. London, England: Academic Press, 2019. ISBN: 0-12-817043-3.
- [17] Erkintalo, M., Genty, G., Wetzel, B. and Dudley, J. Limitations of the linear Raman gain approximation in modeling broadband nonlinear propagation in optical fibers. *Optics express* 18 (Nov. 2010), pp. 25449–60. DOI: 10.1364/OE.18.025449.
- [18] Genty, G. and Dudley, J. M. New approaches to supercontinuum control in the long pulse regime. *Optical Components and Materials VI*. Ed. by S. Jiang, M. J. F. Digonnet, J. W. Glesener and J. C. Dries. Vol. 7212. International Society for Optics and Photonics. SPIE, 2009, 72120J. DOI: 10.1117/12.814721. URL: <https://doi.org/10.1117/12.814721>.
- [19] Husakou, A. V. and Herrmann, J. Supercontinuum Generation of Higher-Order Solitons by Fission in Photonic Crystal Fibers. *Phys. Rev. Lett.* 87 (20 Oct. 2001), p. 203901. DOI: 10.1103/PhysRevLett.87.203901. URL: <https://link.aps.org/doi/10.1103/PhysRevLett.87.203901>.
- [20] Gross, B. and Manassah, J. T. Supercontinuum in the anomalous group-velocity dispersion region. *J. Opt. Soc. Am. B* 9.10 (Oct. 1992), pp. 1813–1818. DOI: 10.1364/JOSAB.9.001813. URL: <https://opg.optica.org/josab/abstract.cfm?URI=josab-9-10-1813>.
- [21] Jin, A., Ze-Feng, W., Jing, H., Liang, G. and Jiang, Z. Coherence properties of the supercontinuum generated in anomalous dispersion region of photonic crystal

- fibers. *Acta Physica Sinica* 61 (Jan. 2012), p. 124211. DOI: 10.7498/aps.61.124211.
- [22] Hamza, M. and Tariq, S. Split Step Fourier Method Based Pulse Propagation Model for Nonlinear Fiber Optics. *2007 International Conference on Electrical Engineering*. 2007, pp. 1–5. DOI: 10.1109/ICEE.2007.4287333.
- [23] Dudley, J. M., Genty, G. and Coen, S. Supercontinuum generation in photonic crystal fiber. *Rev. Mod. Phys.* 78 (4 Oct. 2006), pp. 1135–1184. DOI: 10.1103/RevModPhys.78.1135. URL: <https://link.aps.org/doi/10.1103/RevModPhys.78.1135>.
- [24] Hickstein, D. D., Jung, H., Carlson, D. R., Lind, A., Coddington, I., Srinivasan, K., Ycas, G. G., Cole, D. C., Kowligy, A., Fredrick, C., Droste, S., Lamb, E. S., Newbury, N. R., Tang, H. X., Diddams, S. A. and Papp, S. B. Ultrabroadband Supercontinuum Generation and Frequency-Comb Stabilization Using On-Chip Waveguides with Both Cubic and Quadratic Nonlinearities. *Phys. Rev. Appl.* 8 (1 July 2017), p. 014025. DOI: 10.1103/PhysRevApplied.8.014025. URL: <https://link.aps.org/doi/10.1103/PhysRevApplied.8.014025>.
- [25] Mayer, A. S., Klenner, A., Johnson, A. R., Luke, K., Lamont, M. R. E., Okawachi, Y., Lipson, M., Gaeta, A. L. and Keller, U. Frequency comb offset detection using supercontinuum generation in silicon nitride waveguides. *Opt. Express* 23.12 (June 2015), pp. 15440–15451. DOI: 10.1364/OE.23.015440. URL: <https://opg.optica.org/oe/abstract.cfm?URI=oe-23-12-15440>.
- [26] Lutmirski, R. F. and Buser, R. G. Mutual Coherence Function of a Finite Optical Beam and Application to Coherent Detection. *Appl. Opt.* 12.9 (Sept. 1973), pp. 2153–2160. DOI: 10.1364/AO.12.002153. URL: <https://opg.optica.org/ao/abstract.cfm?URI=ao-12-9-2153>.